Journal of *Marine Science and Engineering*

MDPI

Article

Depositional Setting and Cementation Pattern of Al-Mejarma Beachrocks, Saudi Arabia: A Proxy for the Late Quaternary Red Sea Coastal Evolution

Ibrahim M. Ghandour [1,2,*], Hamad A. Al-Washmi [1], Athar A. Khan [1], Ammar A. Mannaa [1], Mohammed H. Aljahdali [1] and Brian G. Jones [3]

[1] Marine Geology Department, Faculty of Marine Science, King Abdulaziz University, P.O. Box 80200, Jeddah 21589, Saudi Arabia; halwashmi@kau.edu.sa (H.A.A.-W.); geoathar@gmail.com (A.A.K.); amannaa@kau.edu.sa (A.A.M.); maljahdli@kau.edu.sa (M.H.A.)
[2] Geology Department, Faculty of Science, Tanta University, Tanta 31527, Egypt
[3] School of Earth, Atmospheric and Life Sciences, University of Wollongong, Wollongong, NSW 2522, Australia; briangj@uow.edu.au
* Correspondence: ighandour@kau.edu.sa

Abstract: This study utilizes lithofacies characteristics, petrographic, XRD, and stable isotope data of Al-Mejarma beachrocks, Red Sea, Saudi Arabia, to interpret its depositional setting, origin of cement, and coastal evolution. The beachrock is 1.15 m thick, medium to very coarse-grained sandstone with scattered granules. It shows massive to graded bedding, horizontal, ripple, and shore parallel to slightly oblique planar cross-laminations, with a remarkable absence of bioturbation. It was deposited by shore-parallel longshore currents in a relatively high-energy beach environment. The framework comprises quartz, feldspars, and lithic fragments admixed with biogenic remains of algae, mollusca, foraminifera, corals, and echinoids. They are cemented by high magnesium calcite in the form of isopachous rims and pore-filling blades, and rarely, as a meniscus bridge. The mean values of $\delta^{18}O_{VPDB}$ and $\delta^{13}C_{VPDB}$ are 0.44‰ and 3.65‰, respectively, suggesting a seawater origin for the cement. The framework composition, facies geometry, and association with back-barrier lagoon impose a deposition as a shoreface-beach barrier through two stages corresponding to the middle and late Holocene. The first stage attests landward migrating sediment accumulation and rapid marine cementation. The sediments stored offshore during the early and middle Holocene humid periods migrated landward from offshore and alongshore by onshore waves and longshore drift during the middle and late Holocene sea-level highstand. They were cemented to form beachrock and subsequently emerged as the late Holocene sea-level fell.

Keywords: stable isotopes; coastal sand barrier; Red Sea coastal evolution; late Holocene climate and sea level; beachrock petrography

Citation: Ghandour, I.M.; Al-Washmi, H.A.; Khan, A.A.; Mannaa, A.A.; Aljahdali, M.H.; Jones, B.G. Depositional Setting and Cementation Pattern of Al-Mejarma Beachrocks, Saudi Arabia: A Proxy for the Late Quaternary Red Sea Coastal Evolution. *J. Mar. Sci. Eng.* **2021**, *9*, 1012. https://doi.org/10.3390/jmse9091012

Academic Editor: Gemma Aiello

Received: 16 August 2021
Accepted: 13 September 2021
Published: 15 September 2021

1. Introduction

Marine processes play an important role in shaping coastal landforms through the dynamic interplay between geomorphic setting, climate, hydrodynamics, sediment transport, and biogeochemistry [1–5]. The Holocene climate and sea-level changes are the primary drivers of the world's coastal evolution [6]. These changes determine the trends of emergence and submergence, and the formation of several coastal geomorphological features [7–10]. Understanding the past changes in sea level and climate is crucial for effective future long-term and safe coastal development planning [11]. Several proxies including vertical variations in sedimentary facies, upcore fossil and isotopic changes, marine notches, coral reef terraces, and geoarchaeological records have been applied to infer coastal evolution [8,12–14] and sea-level changes [7,10,13,15–17].

Beachrocks are carbonate-cemented sediments of variable composition and grain sizes typically found within the supratidal, intertidal, and upper subtidal zones mostly along

tropical and subtropical coastlines [18–24]. They form during sea-level stillstands or minor regression [7,12]. Various biotic and abiotic processes have been put forward to account for beachrock cementation [20,25,26]. These processes include the mixing of marine and meteoric waters [26], direct precipitation of calcium carbonate in pore spaces as a result of evaporation [27], CO_2 degassing of intertidal groundwater during tidal pumping and spraying [28], and direct or indirect activity of organisms [29,30]. The cement style of beachrocks is affected by coastal zone morphodynamics [31]. Meniscus high Mg-calcite cements grow during the beach phase accretion, when the locus of beachrock formation occurs in the undersaturated sediment in the upper intertidal to supratidal zone, whereas acicular cements form during the landward shift of the beachface, as the beachrocks are exposed to saturated conditions [31]. The texture of the beachrock cement can then reveal short-term cycles of beach progradation and retrogradation [31]. However, such changes may not be apparent where beachrock forms under very arid conditions, such as along the Saudi Red Sea coast.

Beachrocks are widely distributed along the Saudi Red Sea and Gulf of Aqaba coasts [32–36]. Despite their considerable extent, the research on beachrock along the Saudi Red Sea coast is still in earlier stages and is underrepresented. A single published study focused on the cementation patterns, cement composition, and microfabrics of Al-Shuaiba beachrocks [33]. This study showed that the cement consists mainly of aragonite and high Mg-calcite in the form of micritic coatings, isopachous to asymmetric aragonite rim, and cryptocrystalline partial pore-fillings. The cement of the beachrocks of Al-Shuaiba grows selectively around carbonate grains and does not grow around siliciclastic grains. Cement nucleation on carbonate grains was easier as they provide good "seed crystals" for carbonate cement growth [33].

Another interesting beachrock occurrence crops out along the eastern shoreline of the back-barrier Al-Mejarma Lagoon on the Saudi Red Sea coast (Figure 1). It displays sedimentary structures and textural attributes that indicate a high-energy environment and are therefore inconsistent with the low-energy lagoonal system. The present study aims to interpret the depositional setting and the origin of cement in beachrock that is exposed along the eastern coast of Al-Mejarma Lagoon, Central Red Sea, Saudi Arabia, based on field observations, petrography, and carbon and oxygen isotopic data.

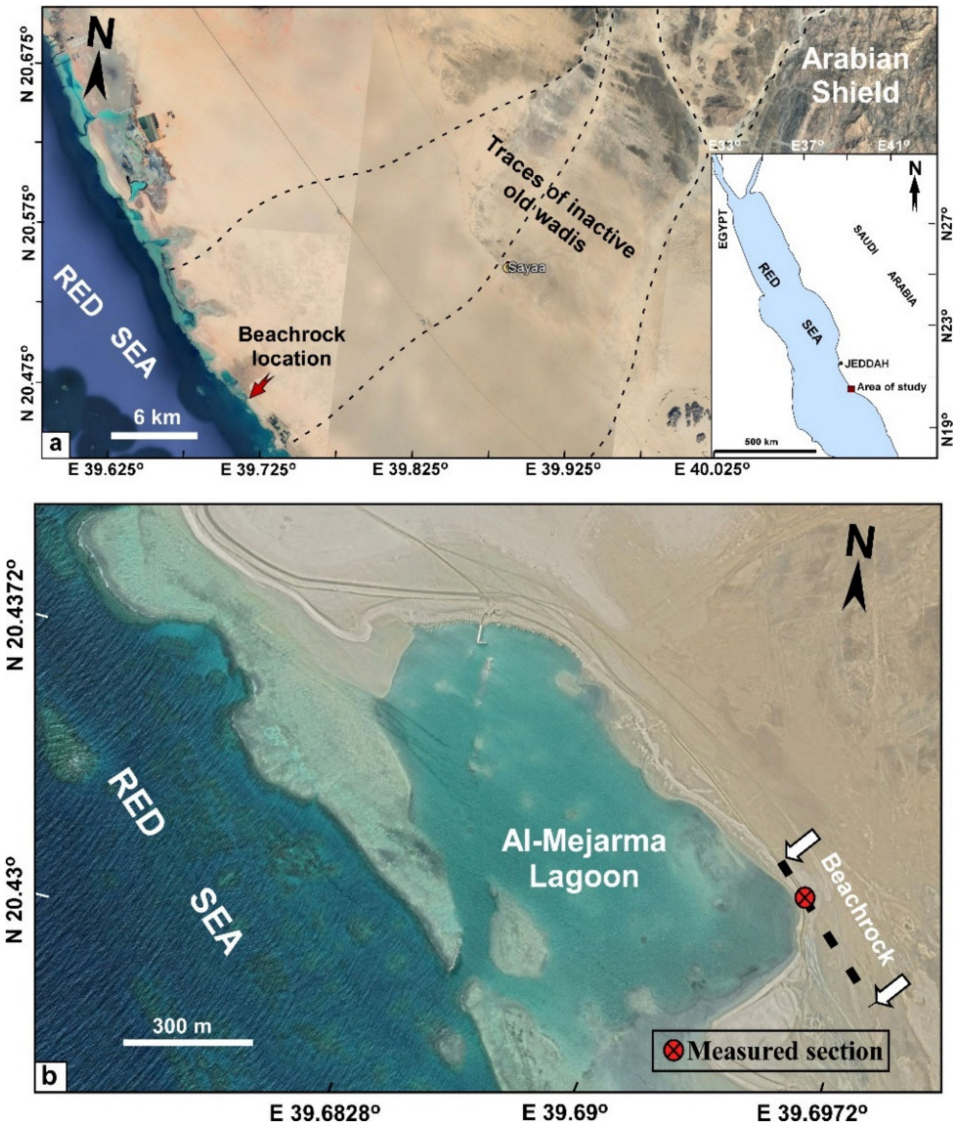

Figure 1. Landsat image showing the location of the area of study: (**a**) Location map of the study area; (**b**) Close up of Al-Mejarma Lagoon showing the extension of the beachrock and the location of the measured section.

2. Holocene Climate and Sea Level in the Red Sea Region

The equatorial regions have experienced a shift in climate and sea level during the Holocene [37,38]. Several unequivocal geological and archaeological archives indicate increased precipitation rates during the early-middle Holocene in the eastern Sahara and Saudi Arabian regions [39–42]. The humid climate was associated with the northward and eastward expansion of the East African Summer Monsoon [42,43]. The humid interval was followed by a progressive increase in aridity during the late Holocene associated with the southward shift of the Intertropical Convergence Zone (ITCZ) [44,45].

The Red Sea region has a generally hot and arid climate throughout the year with low precipitation (<63 mm/y) and high evaporation (2.06 ± 0.22 m/y) rates [46,47]. The Red Sea surface water temperature ranges between 22 and 32 °C [48] and increases from north to the south showing wide variability. In winter, it is 22 °C at the entrance of the Gulf of Suez, about 27 °C at the southern end of the Red Sea and the highest temperature is 28.2 °C recorded at a latitude of N 20°. In contrast, the Red Sea surface water temperature during summer varies from 28 °C at the entrance of the Gulf of Suez to 31 °C at the southern

end of the sea, whereas the highest temperature of 32.5 °C is shifted a little to the south at N 16° [49].

The wave characteristics in the Red Sea area are strongly controlled by the persistent winds that increase the longshore transport [50]. The wind systems of the Red Sea area are dominated by the north-westerly (NNW) wind that blows year-round extending to the southern end of the Red Sea [51]. This wind system generates the most energetic waves in the Red Sea basin. These waves propagate to the southern end of the Red Sea, in the form of swell and frequently as wind sea [52]. In winter (October to April), the NNW winds are restricted to the northern region and the most regular Indian monsoonal winds blow much stronger from SSE to the NNW over the southern and central parts of the Red Sea resulting in the development of a convergence zone at N 20°–25° [46,51,53]. This wind system generates waves that propagate northward and attenuate when they approach the Red Sea's northern end [51]. The Red Sea coast is oriented NNW-SSE, roughly parallel to the prevailing winds, a situation likely to favor longshore currents and littoral drift.

Relative sea-level highstands with spatial, temporal, and amplitude variabilities are recorded during the mid-Holocene (between 7.0 and 4.5 ka), followed by sea-level fall to the present-day level [13,54–59]. Following the last post-glacial sea-level rise, sea-level fluctuations during the Holocene have had a profound influence on the Red Sea's coastal evolution. Evidence for the highstand along the Red Sea and the Gulf of Aqaba coasts is well documented by coral terraces, palaeoshoreline notches, and erosional benches [60–62], shallow subsurface coastal sedimentary facies [63–66] and upcore change in benthic foraminiferal distribution [67,68]. Ghandour and Haredy [64] recognized transgressive-regressive successions from the Red Sea coastal plain of Al-Kharrar Lagoon, Saudi Arabia. The lower transgressive part consisting of gravel-rich fluvial sediments that show an upward increase in marine influence and the overlying lagoonal sediments was attributed to the mid-Holocene relative sea-level rise/highstand. These deposits correspond to the mid-Holocene humid interval [68]. The upper regressive part consists of shallow lagoonal and tidal flat deposits showing features of pedogenesis formed during a phase of sea-level fall under arid climate.

3. Area of Study

Al-Mejarma Lagoon (Figure 1b) is a shallow back-barrier coastal lagoon covering an area of 0.88 km^2 with a maximum water depth of 6 m. It is located between latitudes N 20°25′29″ and N 20°26′4.02″, and longitudes E 39°41′23″ and E 39°42′4″. It is connected to the Red Sea through a shallow (7 m deep) and narrow (70 m width) inlet channel [69,70]. The water dynamic is variable, energetic along the channel, and very calm on both the northern and southern parts of the lagoon. The lagoon has a semidiurnal low tidal range of about 0.3 m that is similar to that of the central Red Sea [71]. The area has no source of freshwater except rare intermittent supply during catastrophic flash floods through occasionally active wadis to the north and south of the area of study.

A low-lying intertidal flat borders the lagoon to the south, to the north and north-east, it is surrounded by coastal dunes, and to the east by beachrocks (Figure 1b). The recent bottom sediments of Al-Mejarma Lagoon are dominated by argillaceous sand and sandy mud; however, coarse bioclastic sediments are abundant along the inlet channel [69,70]. In an ongoing research, a short (2.5 m long) core collected from the intertidal flat shows stacking of two facies; lagoonal gray mud containing skeletal remains of bivalves, gastropods and corals, sharply overlain by intertidal flat yellowish-brown medium-grained sand. This facies organization is consistent with the shallow subsurface coastal facies organization at Al-Shuaiba [67], Al-Kharrar [63,64,68], north Al-Wajh [65], and Al Lith [66].

The terrigenous influx into the lagoon was derived from the volcanic and sedimentary rocks of the Al Lith belt [72]. The belt generally consists of basalt, andesite, and dacitic tuff interbedded with and overlain by volcaniclastic and epiclastic rocks, and thin marble and chert beds [73]. Since extreme aridity developed in the late Holocene, most wadis eventually became inactive and the sediment supply to the coast ceased (Figure 1a).

4. Materials and Methods

Beachrocks are best exposed on the eastern coast of the Al-Mejarma Lagoon, Saudi Arabia (Figure 1). Laterally, they are poorly exposed, with only the upper surface exposed while the rest is hidden within intertidal flat deposits. A sedimentary log (Figure 2) was measured, described, and samples were collected from the exposure on the lagoonal coast. The elevation above the mean sea level (MSL) was determined using a Leica Viva GNSS GS15 receiver. Different lithofacies were identified based on texture and sedimentary structures. Seven thin sections were prepared in the Laboratory of Petrology, Geology Department, Cairo University, Egypt. The original samples were cut into 3 × 2 cm chips perpendicular to the bedding plane. The chips were then mounted on a glass slide using Canada balsam, and after drying it, is polished to a thickness of 0.03 mm. The thin sections were investigated by a polarizing microscope to determine framework composition, texture, and cement morphology. The bulk mineralogical composition was determined using X-ray diffraction (XRD) analysis. A gram of each dry sample was powdered using an agate mortar and pestle, and the powdered sediment was packed into a cavity-bearing slide, which was scanned from 2–40° 2θ at speed of 1°/min. To convert X-ray peak angles to percentage of magnesium (in mol% of $MgCO_3$) in the calcite lattice, the chart suggested by Goldsmith et al. [74] was used. Stable isotopic values of $\delta^{18}O$ and $\delta^{13}C$ in the carbonate cement were measured using an automated carbonate preparation device (KIEL-III) coupled to a gas-ratio mass spectrometer (Finnigan MAT 252) at the Environmental Isotope Laboratory, Geosciences Department, University of Arizona. The cement was separated using a micro-drill to avoid contamination. Powdered samples were reacted with dehydrated phosphoric acid under vacuum at 70 °C. The isotope ratio measurement is calibrated based on repeated measurements of international reference materials (NBS-19 and NBS-18) and precision is ±0.10‰ for $\delta^{18}O$ and ±0.08‰ for $\delta^{13}C$ (1 sigma). The isotopic values are reported relative to the Vienna Pee Dee Belemnite (VPDB) international standard [75]. To distinguish the type of porewater from which the carbonate cement is precipitated, the Z value [76] is calculated as follows:

$$Z = a\ (\delta^{13}C + 50) + b\ (\delta^{18}O + 50)$$

where a and b are constant values equal to 2.048 and 0.498, respectively. Z values > 120 indicate a cement of marine water origin, whereas values <120 suggest a cement of freshwater origin. The morphology and microstructures of the cement were examined using scanning electron microscopy (5 kV accelerating voltage, SEM-EDS, JSM-6360 LA, JEOL) at Kafrelsheikh University, Egypt. The Mg mass % of the cement was determined for two samples (HMD3 and HMD7) using EDX.

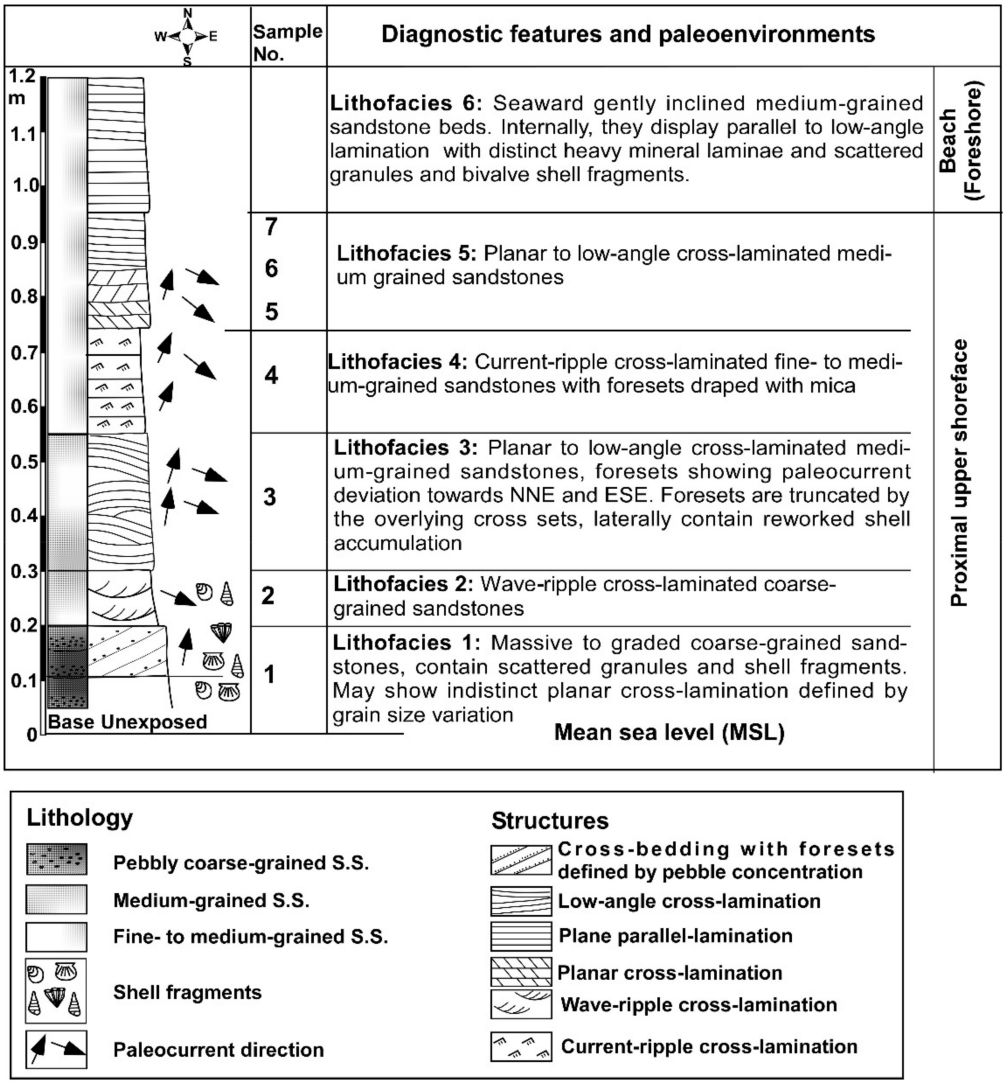

Figure 2. The sedimentary log, location of analyzed samples, and the lithofacies characteristics that were recognized from the Al-Mejarma beachrock (see Figure 1 for location).

5. Results

An interesting beachrock crops out along the eastern shoreline of Al-Mejarma Lagoon displaying relatively high-energy sedimentary structural and textural attributes. It extends for 400 m in a NNW-SSE direction parallel to the Red Sea shoreline and about 7 m inland with a thickness of 1.15 m (Figures 2 and 3a). The composition and texture of the beachrock are texturally and compositionally different from the surrounding lagoonal and tidal flat unconsolidated sediments.

Figure 3. Field photographs showing the characteristic features of the beachrock of the Al-Mejarma: (**a**) An overview of strike and inland extension of Al-Mejarma beachrock. This part shows the seaward inclined foreshore sandstones (lithofacies 6); (**b**) General overview showing breakdown and sliding of beachrocks due to modern wave erosion. The person is 1.7 m tall; (**c**) Coarse-grained pebbly sandstones of lithofacies 1 overlain by wave ripple cross-laminated sandstones of lithofacies 2; (**d**) Low-angle cross-lamination of lithofacies 3; (**e**) Ripple cross-laminated (lithofacies 4) showing foresets draped by mica and foresets dipping toward N and NNE, and low-angle planar cross-laminated medium-grained sandstones of lithofacies 5 with foresets trending SSE, and (**f**) Low-angle tabular cross-laminated medium-grained sandstones of lithofacies 5. Note the current directions towards SSE and NNE. The scale is hammer = 0.33 m, pen in (**d**–**f**) = 0.14.

5.1. Morphology and Lithofacies

The beachrock occurs from 1.2 m above the mean sea level (MSL) in the form of tabular horizontal to slightly inclined cemented horizons. The cemented beachrock horizons consist of massive, planar, and ripple cross-laminated sand with foresets trending parallel to slightly oblique to the Red Sea coastline (Figure 3a,b). Textural characteristics and sedimentary structures were used to subdivide the studied beachrocks into six vertically stacked lithofacies (Figure 2). Lithofacies 1 is defined from the base of the beachrock successions. It is about 0.15 m thick and consists of sharp-based massive to normal graded, poorly sorted, coarse- to very coarse-grained sandstone containing dispersed granules of

lithic fragments and skeletal remains (Figure 3c). The basal part is substantially coarser. Laterally, it shows indistinct planar cross-laminations defined by variations in grain size. Lithofacies 2 consists of a 0.1 m thick sharp-based, wave ripple cross-laminated, moderately sorted, coarse-grained sandstone (Figure 3c). Lithofacies 3 is about 0.25 m thick, planar-laminated to low angle cross-laminated, moderately sorted, medium- to coarse-grained sandstone (Figure 3d).

Lithofacies 4 consists of a 0.2 m thick, moderately well-sorted, medium-grained sandstone, displaying current ripple cross-laminations with foresets dipping to N and NNE defined by mica concentrations (Figure 3e). Lithofacies 5 consists of a 0.2 m thick, moderately well-sorted, medium-grained sandstone displaying small scale planar tabular to low-angle cross-stratification with foresets showing paleo flows towards NNE and SSE (Figure 3e,f). Lithofacies 6 occupies the upper part of the beachrock exposure showing gently inclined geometry dipping about 9° towards the west (seaward). It consists of a 0.25 m thick, plane to low-angle parallel-laminated, moderately well-sorted, medium- to coarse-grained, occasionally pebbly sandstone with foresets defined by heavy mineral laminae (Figure 3a).

5.2. Framework Composition and Cement

The framework composition includes mixed siliciclastic and biogenic calcareous grains of variable sizes ranging from silt to granule size (Figure 4). Siliciclastic grains are dominated by quartz: mono- and polycrystalline, silt to gravel size, angular to well-rounded grains. Feldspars are the second most abundant siliciclastic grains including both K-feldspars and plagioclase (Figure 4a,b). In addition, relatively rare biotite, amphiboles, heavy minerals, and basaltic and chert lithic fragments are recorded. The skeletal remains are dominated by coralline algae and benthic foraminifera (Figure 4a,b). Remains of bivalves, gastropods, echinoids, corals, and ostracods occur with relatively low abundance. The $CaCO_3$ content of the bulk samples (Table 1) varies between 31 and 68% (mean 48%). The XRD analysis shows that the bulk mineral composition is dominated by quartz, plagioclase, K-feldspars and high Mg-calcite (mol% of $MgCO_3$ varies between 13 and 16%), and traces of amphiboles. EDX analysis of the cement shows that the Mg mass % in samples HMD3 and HMD7 are 3.55 and 0.72%, respectively. High Mg-calcite (HMC) cement occurs dominantly as pore-filling and isopachous rims around grains (Figure 4c,d), and rarely as microcrystalline meniscus bridges linking grains (Figure 4b). It occurs as subhedral to euhedral crystals, which may have a blade-shape and scalenohedral forms (Figure 5a–d). The scalenohedral crystals in the upper part have a morphology that exhibits dissolution features such as corroded or cracked surfaces (Figure 5e,f).

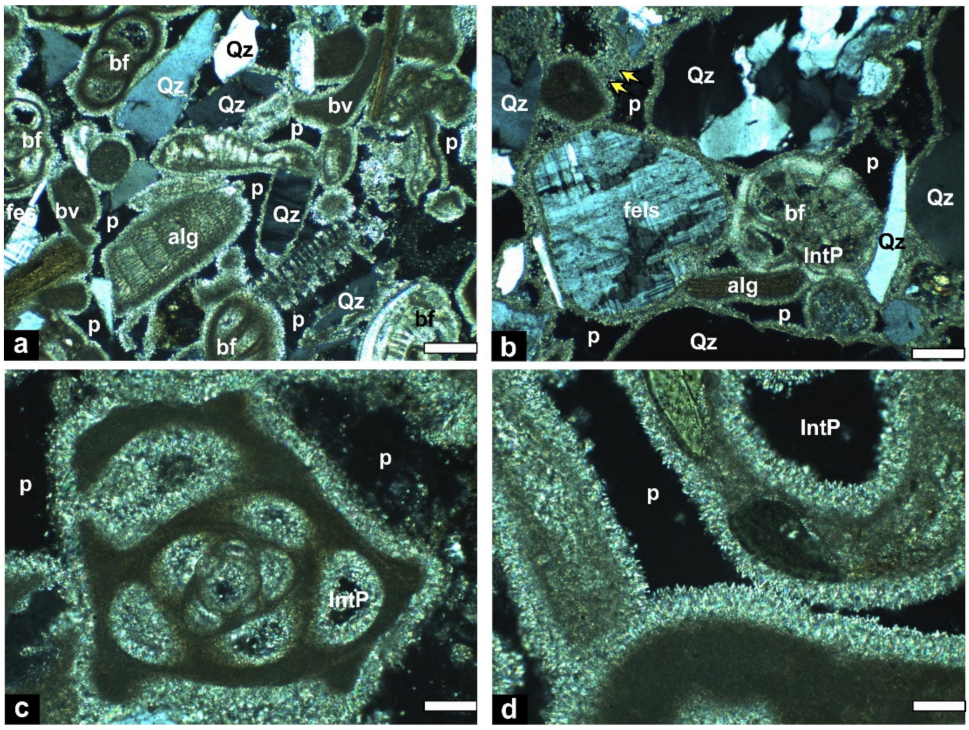

Figure 4. Photomicrographs showing the framework composition and the cement in the beachrock of Al-Mejarma: (**a**,**b**) Varieties of siliciclastic grains dominated by mono- and polycrystalline quartz (Qz) and feldspar (fels) mixed with skeletal remains dominated by benthic foraminifera (bf), coralline red algae (alg), bivalves (bv), and intergranular pores (p); the grains are cemented by HMC mainly in the form of isopachous rims and rarely as microcrystalline meniscus bridge between grains (yellow arrow); (**c**,**d**) HMC cement grows as isopachous fringes with elongated bladed crystals regularly surrounding skeletal remains and filling the intragranular pore (IntP) in the foraminifera test. (The scale bar in (**a**,**b**) = 200 μm and in (**c**,**d**) = 40 μm).

Table 1. The $CaCO_3$ content of the bulk beachrock samples and stable isotope, and Z values of carbonate cement in the Al-Mejarma beachrock. The isotopic values are normalized to Vienna Pee Dee Belemnite (VPDB).

Sample	$CaCO_3$ %	$\delta^{13}C_{VPDB}$	$\delta^{13}O_{VPDB}$	Z
7	68	3.64	0.54	135.0
6	31	3.75	0.31	135.1
5	54	3.78	0.10	135.1
4	52	3.88	0.68	135.6
3	51	3.48	0.37	134.6
2	48	3.32	0.33	134.3
1	36	3.65	0.73	135.1
Min	31	3.32	0.10	134.26
Max	68	3.88	0.73	135.58
Mean	48	3.65	0.44	134.98

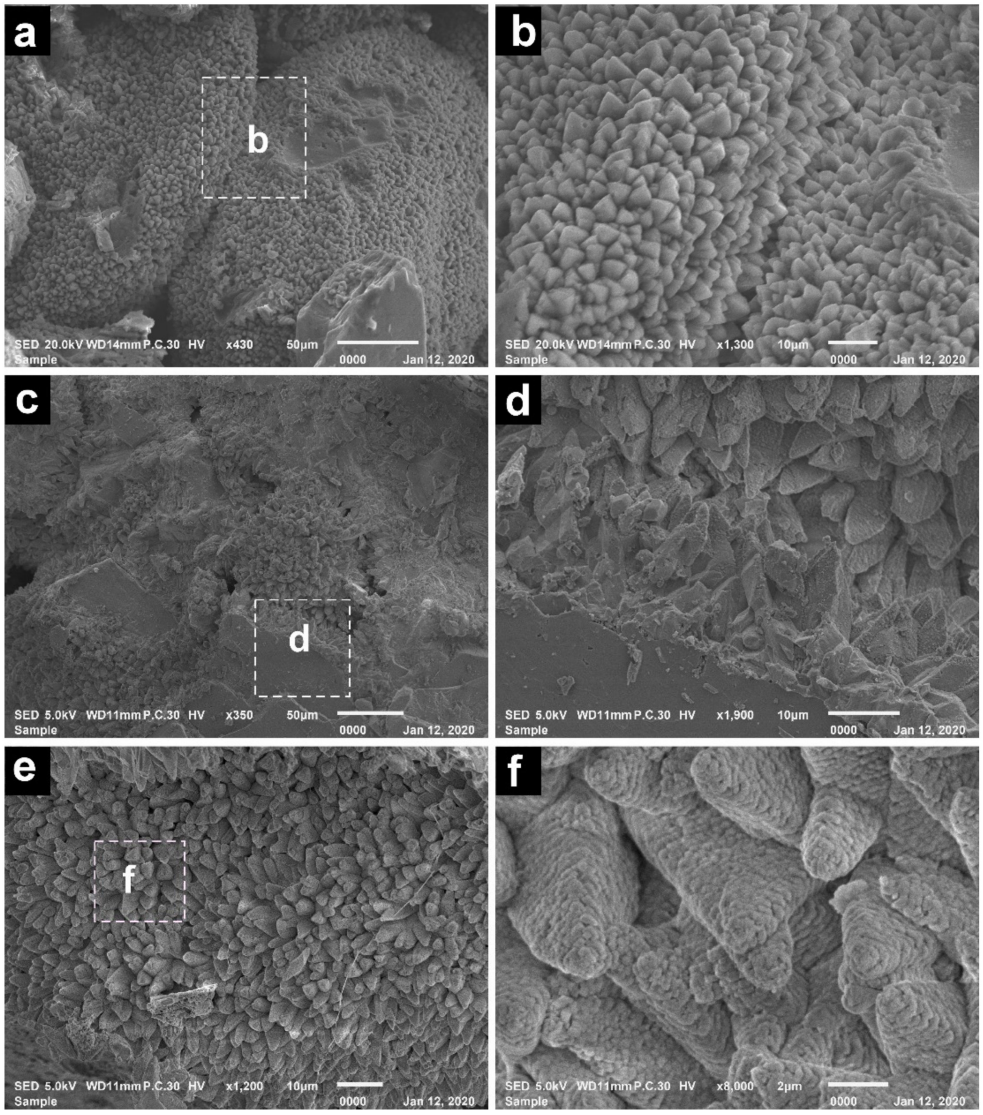

Figure 5. SEM photomicrographs showing the characteristic features of the HMC cement in the beachrock of Al-Mejarma: (**a**,**b**) Isopachous rim with scalenohedral HMC crystals; (**c**–**f**) HMC cement with bladed morphology, with crystal showing dissolution features of rounded corroded crystal outlines in HMD7 (**e**,**f**).

5.3. Oxygen and Carbon Isotopic Data

Stable isotope ($\delta^{13}C$ and $\delta^{18}O$) data for the seven studied beachrock samples are shown in Table 1. Generally, the $\delta^{13}C_{VPDB}$ values of calcite cement vary between 3.32‰ and 3.88‰ (mean 3.65‰), and the $\delta^{18}O_{VPDB}$ values range from 0.10‰ to 0.73‰ (mean 0.44‰). The calculated Z values for the Al-Mejarma beachrocks range from 134.3 to 135.6 (Table 1) indicating a marine origin for the cement.

6. Discussion

The calcareous sandbody bordering the eastern shoreline of Al-Mejarma Lagoon displays cross-lamination, a medium to coarse grain size, with granules and shell fragments indicating a relatively high-energy marginal marine depositional setting [77], which contrast with the adjacent low-energy lagoonal environment. It suggests that the geometry of the paleo-coastline at the time of the sandbody formation was different compared to the current situation. As discussed in the following sections, the elongated, coast-parallel geometry, texture, framework composition, and the bladed and cryptocrystalline high Mg-calcite cements of marine origin, all point to a beachrock origin [19,20].

6.1. Depositional Setting

The shoreline aligned sandbody, the lithofacies characteristics, the absence of fine-grained sediments, and the presence of reworked shell fragments suggest deposition either as prograding upper shoreface-beach deposits of a strandplain or a coastal barrier spit/island [2,4–6,78–80]. Coastal barriers and strandplains are prominent depositional features supplied and molded almost entirely by marine processes. They consist of sandbodies of similar origin and facies characteristics. They are highly dynamic and show significant facies variability even within minimal thicknesses [1,80]. Contrary to strandplains, coastal barriers are elongate sandy islands, of different width, parallel to the shore and separated from the mainland by lagoons [81]. The association of the present beachrock with a back-barrier lagoon (Al-Zubeiri, pers. comm. 2021) excludes a strandplain origin [82]. Beachrocks on barrier island/spits are not recorded from the Red Sea, whereas beachrocks associated with a strandplain are recognized from Al-Shuaiba [33].

The formation and evolution of coastal barriers/spits are largely controlled by availability of mobile sediments, hydraulic (wave and tide) energy, sea-level (SL) changes and a low-gradient profile to provide space for a back-barrier lagoon to form [4,5,78,80,83–85].

6.2. Source and Availability of Sediments

The composition and the availability of sediments for building coastal barriers depend largely on the regional geology and climate. Modern-day siliciclastic barriers are recognized from humid regions covering about 12 to 13% of the world's coasts [6,78,80], whereas carbonate barriers are developed under arid to semi-arid climate comprising only 1% [4]. Barriers develop when the supply of bulk sediments from alongshore or offshore sources are plentiful. The source of sediments needed for building barrier island/spits vary widely. The sediments of some barriers, such as Provincelands Spit in northern Cape Cod, Massachusetts, and Lawrencetown barrier along the northeast shore of Nova Scotia, may be derived from eroding headlands [86,87]. The late-Holocene carbonate spits at Al Dakhirah, Qatar, Arabian Gulf, were derived from the erosion of shore-parallel reefal materials seaward and from the downdrift 'headland' [4]. The sediments for barrier systems may also be derived from the inner continental shelf or derived directly from rivers. For example, Sloss et al. [88] suggested that the sediments which built the barrier estuary system in the Lake Illawarra, New South Wales, Australia, were derived from sediments stored on the continental shelf during the last glacial sea-level fall. In addition, an inner shelf source of reworked cool-water biogenic sediments was recognized for barrier construction in South Australia [89].

The framework composition of the Al-Mejarma beachrock consists of a mixture of calcareous skeletal remains, representing communities living in the inner shelf, and land-derived siliciclastic terrigenous sediments that were discharged offshore from the surrounding catchment. In the area of study, there is no preserved headland on the downdrift side and siliciclastic detritus was derived from the Al-Lith volcanic belt in the hinterland to the east. Thus, the beachrock composition reflects a period of sediment availability, coastal zone morphology, lagoonal extension, and hydrodynamic forcings different from the current situation.

The modern nearshore area receives very little or negligible terrigenous sediments because of the extremely arid climate and the very low precipitation rates and runoff, which are unable to activate wadis [90]. Therefore, the coarse siliciclastic sediments in the beachrocks must have been discharged into the coastal area during a period of relatively higher precipitation rates and greater runoff compared to the present-day climatic conditions. This humid interval may be correlated with the early-middle Holocene period [39,90]. The mid-Holocene humid climate with an annual monsoonal precipitation rate of 400 mm/y was recorded by geological and geoarchaeological features in Arabia and North Africa [40,61]. During this humid interval, floods may have been more frequent than they are today, and were perhaps capable of carrying a huge amount of siliciclastic sediment to be discharged into the offshore. The sediments that were delivered are

medium- to very coarse-grained, occasionally pebbly, and mineralogically and texturally submature. Therefore, the heterogeneous composition of the beachrock suggests that the terrigenous siliciclastic sediments spent significant time on the inner shelf and mixed with autochthonous calcareous biogenic sediments. These sediments were later transported shoreward by energetic flows from offshore and by onshore and longshore drifts, and they migrated landward forming a shoreface-beach barrier bordering the Al-Mejarma Paleolagoon during the middle and late Holocene sea-level highstand and fall.

6.3. Sediment Transportation and Deposition

Onshore and alongshore sediment transport that is necessary for the formation of barrier systems is significantly controlled by hydrodynamic wave energy and wave-induced currents [91]. Although rare, barrier systems are recognized from hypertidal coasts [91], whereas they typically characterize microtidal coasts with wave heights less than 2 m [92]. The Red Sea coast is suitable for the formation of coastal barriers because of its limited tidal range and average wave height (<2 m). The sediments of the Al-Mejarma beachrock lack sedimentological size alternation reflecting stability in sediment supply and almost continuous sediment transport. In such an arid region, the study area lacks perennial streams and, therefore, contemporaneous supply by longshore drift from deltas at the mouths of wadis is also excluded. Instead, the stored offshore sediments were moved onshore from the inner shelf during long-term accretionary wave conditions. In contrast, the formation of coastal barriers in humid regions suggest a continuous longshore supply of river mouth coarse siliciclastic sediments [78,80]. In this setting, the onshore movement of sediments that come from the inner shelf, is much less efficient than alongshore movement because normal fair-weather wave action is thought to preferentially move sediment onshore from relatively shallow depths (i.e., the upper shoreface [89,93,94]).

Sedimentary structures and bedding style in the Al-Mejarma beachrock indicate deposition in an upper shoreface to beach environment with the role of wind-generated waves and currents as driving forces for sediment transport and deposition. Graded beds with sharp erosive base together with wave rippled, horizontal to slightly inclined planar laminated coarse-grained sandstones (lithofacies 1–3) strongly indicate high-energy storm events. Cross-lamination with foresets trending parallel to or slightly oblique to the Red Sea shoreline (lithofacies 4 and 5) were formed by the migration of straight-crested megaripples in the surf (upper shoreface) zone by longshore flow [95]. The gently seaward inclined strata, planar, and low-angle stratifications with foresets defined by heavy minerals suggest deposition of lithofacies 6 by wave swash and backwash in the foreshore [77,96].

The major depositional processes operating on barrier systems are wind-driven waves [97]. When waves approach shorelines obliquely, they generate longshore currents, which transport sediments parallel to the shoreline, and form spits and barrier islands [78,97]. As the wind systems change seasonally, the direction of wave approach and resulting longshore current systems also change seasonally [97,98]. Measured paleo flow trends in the Al-Mejarma beachrock are largely towards NNE and SSE parallel to slightly oblique the Red Sea shoreline. This trend reflects the direction of the longshore flow following the direction of wind stresses. The prevailing winds from the NNW in summer would have generated appreciable and significant SSE longshore drift that was capable of transporting sediments towards SSE. The wind direction is reversed in winter and the southern and central Red Sea regions up to latitudes of N 20–25° are strongly influenced by the strong Indian monsoon-related SSE winds [53]. As a result of the southerly monsoon-related winds, there would have also been a strong net sediment transport northward producing NNE-trending cross-beds.

6.4. Sea Level and Climate Controls

The Holocene sea level and climate changes played a significant role in the formation of the barrier system and the coastal evolution at Al-Mejarma. Sea-level changes regulated sediment dispersion, transportation, and shoreline trajectory, whereas climate controlled

sedimentation rate. The Al-Mejarma area was subaerially exposed during the Last Glacial Maximum (LGM), and was subsequently inundated by the post glacial rapid sea-level rise as the sea level rose to its present level or slightly higher during middle Holocene [56,61,99]. The humid mid-Holocene period coincided with a relative sea-level highstand as reported in many localities in the Red Sea area [61,64,90]. The sea level was 0.5–1.0 m higher than its present level [61,99], which accounts for the raised elevation of the Al-Mejarma beachrock. Hein et al. [61] reported marine notches and terraces as well as coral reef terraces of the mid-Holocene age along the Egyptian Red Sea coast suggesting a highstand of 1.1 to 1.8 m above mean sea level. Huge amounts of siliciclastic sediments of different grain sizes would have been transported to the inner shelf through wadis during this early to middle Holocene humid period.

Durgaprasada Rao and Behairy [90] attributed the abrupt cessation of coarse siliciclastic input into the Red Sea coast and subaerial exposure of reef flats to the change of climate from humid to arid and a drop of sea level by about one meter. Prograding barrier systems form in a regime of abundant sand supply during a period of sea-level highstand and fall [79,88,100,101]. The late Holocene climate became extremely arid and the wadis turned inactive. The sediments that were initially dispersed in the proximal continental shelf were transferred toward the shoreline by wave action during the transgressive phase, in what was termed a cannibalistic process [85,102].

The framework composition, lithofacies characteristics, and cementation suggest that the formation of Al-Mejarma beachrock has been accomplished through two evolutionary stages (Figure 6a–c) in response to the interplay of the Holocene climate and sea-level changes. During the middle Holocene sea-level highstand and late Holocene sea-level fall, continued onshore migration of stored inner shelf sediments forced coastal progradation, provided a nucleation site for the paleo-barrier system, and caused seaward shoreline movement (Figure 6a,b). Al-Mejarma Paleolagoon formed and developed simultaneously with or after barrier formation. Continuous coastal progradation and sea-level fall during the late Holocene led to a major rearrangement of the depositional system, a gradual reduction and abandonment of the back-barrier lagoon leaving a lowland area that is filled with the present-day tidal flat deposits, while a new barrier and lagoon developed seaward of the old barrier coast and beachrock (Figure 6c).

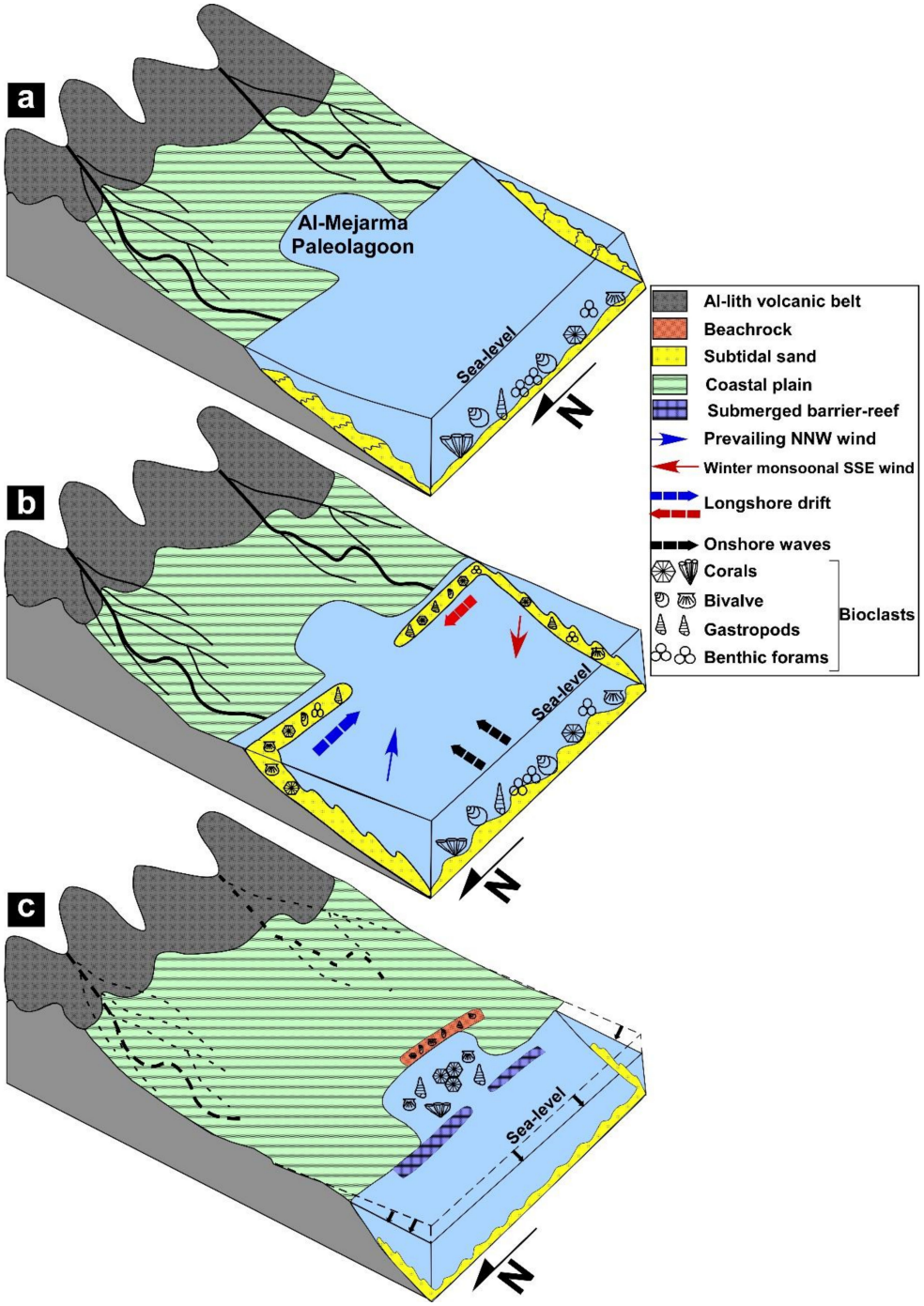

Figure 6. Al-Mejarma coastal evolution and depositional model of beachrock formation: (**a**) A landward extension of Al-Mejarma Lagoon following the post-glacial sea-level rise, where lowland coastal areas were flooded; (**b**) A huge amount of siliciclastic terrigenous sediments were injected through wadis to the north and south into the Red Sea coastal area and offshore. The sediments were prograded landward by the action of onshore waves and longshore drift building a shoreface-beach barrier during mid-Holocene sea-level highstand; (**c**) Finally, the shoreface-barrier sediments were emerged, cemented, and the lagoon shrunk to it its current position following the late Holocene relative sea-level fall and intensive arid climate.

6.5. Origin of Cement

Rapid cementation processes enhance the preservation of beachrock [103]. High-energy wave and current conditions and the relatively coarse, porous, and per-

meable sediments facilitate the free circulation of seawater allowing supersaturated marine water to move through the pore system, and helped to precipitate the cement [104].

Petrographic and SEM examinations, XRD data, and the isotopic values of the cement in the Al-Mejarma beachrock suggest that the regular distribution of isopachous HMC cement showing prismatic fringes and small equant crystals suggest precipitation exclusively in a marine phreatic environment [105–107]. In contrast to more humid coastal beachrock [31], there is no evidence at Al-Mejarma for cementation within the meteoric environment [105,106,108]. Magnesium calcite cement favors precipitation from seawater, and lithification either occurs at depth after percolation or seawater evaporation [109]. Similar isopachous rims of HMC blade cement have been documented from the beachrocks of the Arabian Gulf [110]. The rare occurrence of meniscus cement suggests a subtidal environment [111].

Carbon and oxygen stable isotopes, in combination with petrographic characteristics, have been widely utilized to trace the source of carbonate cement and to interpret the diagenetic environment and processes of beachrock formation [15,18,107,112–114]. The $\delta^{13}C$ values from the beachrock cement are consistent with the values of marine carbonates [115]. The water from which the cement was derived has relatively homogeneous temperature and uniform composition as shown by observed isotopic homogeneity of the studied samples [18,108]. The $\delta^{18}O$ isotopes of carbonates normally reflect the temperature, salinity, and isotopic composition of the fluid from which they precipitate, thus freshwater carbonates possess negative $\delta^{18}O$ values whilst marine cement shows positive values [104]. The positive values correlate well with cement precipitated under the seawater environment [104]. A low average value of $\delta^{18}O$ (0.5‰), similar to the cement data obtained in the present study, was reported by Holail and Rashed [18] in the Mediterranean and the Red Sea. The Z values for the Al-Mejarma beachrocks range from 134.3 to 135.6, suggesting that the cement was generated predominantly from seawater [76]. This is similar to the average Z value of 135 from the Holocene beachrock in northeastern Brazil that also indicates dominantly marine cementation [23].

The mild modifications of the initial cement fabrics by etching and dissolution features observed in the upper part of the beachrock sequence (Figure 5e–f) are possibly related to rare rainstorms or desert dew. The beachrocks were not exposed to pervasive meteoric diagenesis. However, calcite cements showing signs of dissolution and depletion of their Mg content in the upper part of the beachrock profile have been attributed to the effect of infiltration of meteoric water and subaerial exposure [12,16,17,24].

The Al-Mejarma coastal evolution is in agreement with previous barrier island systems [88]. The results from this study add greater detail to the development of a beach barrier system in arid regions. Though the shortcoming of the present study is the lack of precise dating of the beachrocks, their formation is probably associated with the mid to late Holocene sea-level and climate changes. The initiation of many modern coastal barrier-lagoon systems worldwide is linked to the deceleration of sea-level rise and initial fall between 7000 and 4000 BP [116]. The cementation of Al-Mejarma beachrock may be correlated with the nearby Al-Shuaiba beachrocks (about 40 km to the north of Al-Mejarma). The beachrocks of Al-Shuaiba also occur at an elevation of 1.2 m above mean sea level and dated back as 3160 $\pm$ 110 years BP [117].

7. Conclusions

The Al-Mejarma beachrock geometry, orientation, and lithofacies characteristics pertain to an upper shoreface to foreshore barrier system formed by onshore and longshore migration of sand. The framework composition includes mixed siliciclastic and calcareous biogenic grains of variable grain sizes, ranging from medium sand to granule, cemented by high Mg-calcite. The cement occurs mainly as an isopachous rim around grains, pore-filling with scalenohedral and blade-shaped crystals, and rarely forms a meniscus bridge between grains. The cement developed mainly under marine phreatic conditions and the uniform $\delta^{18}O$ isotopic and $\delta^{13}C$ values of the cement suggest that the cement was derived

mainly from seawaters of constant composition and temperature. The scalenohedral crystals in the upper part of the beachrock exhibit dissolution features possibly related to the rare rainstorms and desert dew.

The coastal evolution and the formation of the Al-Mejarma beachrock reflect the effect of the Holocene sea-level and climate changes. During the early-middle Holocene humid interval, huge amounts of siliciclastic sediments were transported through wadis from the Arabian Shield and stored offshore. These siliciclastic sediments along with shallow marine calcareous skeletal remains migrated shoreward to the east, SSE, and NNE by wind-generated onshore waves and longshore drift to form a barrier island/spit in the Al-Mejarma area during the middle and late Holocene sea-level highstand and fall. The beachrock sediments were preserved by rapid marine cementation. The late Holocene sea-level fall, and a progressive increase in aridity, led to the emergence of the shoreface-beach barrier. In addition, the Al-Mejarma Paleolagoon was gradually infilled, becoming shallower and closed, while a new lagoon formed seaward of the beachrock.

Author Contributions: Conceptualization, I.M.G., H.A.A.-W. and A.A.K.; methodology, I.M.G., A.A.M. and M.H.A.; software, I.M.G.; validation, I.M.G., H.A.A.-W. and A.A.K.; formal analysis, I.M.G.; investigation, I.M.G., A.A.M., M.H.A.; resources, I.M.G.; data curation, I.M.G. and B.G.J.; writing—original draft preparation, I.M.G., H.A.A.-W., A.A.K.; writing—review and editing, I.M.G. and B.G.J.; supervision, H.A.A.-W.; project administration, I.M.G.; funding acquisition, I.M.G. All authors have read and agreed to the published version of the manuscript.

Funding: This project was funded by the Deanship of Scientific Research (DSR) at King Abdulaziz University, Jeddah, grant number G-312-150-37.

Institutional Review Board Statement: Not applicable.

Informed Consent Statement: Not applicable.

Data Availability Statement: The study did not report any data.

Acknowledgments: This project was funded by the Deanship of Scientific Research (DSR) at King Abdulaziz University, Jeddah, under grant number G-312-150-37. The authors thank the DSR for this technical and financial support. The authors are grateful to Maurice Tucker (Univ. of Bristol) for the fruitful discussion about the cement and depositional setting. We extend our thanks to Essam Aboud, Aaid Al-Zubeiri, and Bandar Al-Zahrani (King Abdulziz University) for their assistance in field work. We are very grateful to the editor and the reviewers for their constructive comments and editorial handling.

Conflicts of Interest: The authors declare no conflict of interest.

References

1. Anthony, E.J. Wave influence in the construction, shaping and destruction of river deltas: A review. *Mar. Geol.* **2015**, *361*, 53–78. [CrossRef]
2. Forde, T.C.; Nedimović, M.R.; Gibling, M.R.; Forbes, D.L. Coastal evolution over the past 3000 years at Conrads Beach, Nova Scotia: The influence of local sediment supply on a paraglacial transgressive system. *Estuaries Coasts* **2016**, *39*, 363–384. [CrossRef]
3. Falkenroth, M.; Adolphs, S.; Cahnbley, M.; Bagci, H.; Kázmér, M.; Mechernich, S.; Hoffmann, G. Biological indicators reveal small-scale sea-level variability during MIS 5e (Sur, Sultanate of Oman). *Open Quat.* **2020**, *6*, 1–20. [CrossRef]
4. Rivers, J.; Engel, M.; Dalrymple, R.; Yousif, R.; Strohmenger, C.J.; Al-Shaikh, I. Are carbonate barrier islands mobile? Insights from a mid to late-Holocene system, Al Ruwais, northern Qatar. *Sedimentology* **2020**, *67*, 534–558. [CrossRef]
5. Mulhern, J.S.; Johnson, C.L.; Green, A.N. When is a barrier island not an island? When it is preserved in the rock record. *Front. Earth Sci.* **2021**, *8*, 560437. [CrossRef]
6. Hein, C.J.; Fitzgerald, D.M.; Cleary, W.J.; Albernaz, M.B.; de Menezes, J.T.; Klein, A.H.D.F. Evidence for a transgressive barrier within a regressive strandplain system: Implications for complex coastal response to environmental change. *Sedimentology* **2013**, *60*, 469–502. [CrossRef]
7. Cooper, J.A. Beachrock formation in low latitudes: Implications for coastal evolutionary models. *Mar. Geol.* **1991**, *98*, 145–154. [CrossRef]
8. Dickinson, W.R. Paleoshoreline record of relative Holocene sea levels on Pacific islands. *Earth-Sci. Rev.* **2001**, *55*, 191–234. [CrossRef]

9. Harvey, N. Holocene coastal evolution: Barriers, beach ridges, and tidal flats of South Australia. *J. Coast. Res.* **2006**, *22*, 90–99. [CrossRef]
10. Kelly, C.S.; Green, A.N.; Cooper, J.A.G.; Wiles, E. Beachrock facies variability and sea level implications: Preliminary study. *J. Coast. Res.* **2014**, *70*, 736–742. [CrossRef]
11. Duong, N.; Lieu, N.T.; Cúc, N.T.; Saito, Y.; Hương, N.T.; Phượng, N.T.; Thuy, A.H. Holocene paleoshoreline changes of the Red River Delta, Vietnam. *Rev. Palaeobot. Palynol.* **2020**, *278*, 104235. [CrossRef]
12. Erginal, A.E. Beachrock as evidence of sea-level lowstand during the Clasical period, Parion antique city, Marmara Sea, Turkey. *Geodin. Acta* **2012**, *25*, 96–103. [CrossRef]
13. Stattegger, K.; Tjallingii, R.; Saito, Y.; Michelli, M.; Thanh, N.T.; Wetzel, A. Mid to late Holocene sea level reconstruction of southeast Vietnam using beachrock and beach-ridge deposits. *Glob. Planet. Chang.* **2013**, *110*, 214–222. [CrossRef]
14. Öztürk, M.Z.; Erginal, A.E.; Kiyak, N.G.; Öztürk, T. Cement fabrics and optical luminescence ages of beachrock, North Cyprus: Implications for Holocene sea-level changes. *Quat. Int.* **2016**, *401*, 132–140. [CrossRef]
15. Spurgeon, D.; Davis, J.R.A.; Shinn, E.A. Formation of 'beachrock' at Siesta Key, Florida, and its influence on barrier island development. *Mar. Geol.* **2003**, *200*, 19–29. [CrossRef]
16. Erginal, A.E.; Ekinci, Y.L.; Demirci, A.; Bozcu, M.; Ozturk, M.Z.; Avcioglu, M.; Oztura, M.Z. First record of beachrock on Black Sea coast of Turkey: Implications for late Holocene sea-level fluctuations. *Sediment. Geol.* **2013**, *294*, 294–302. [CrossRef]
17. Mauz, B.; Vacchi, M.; Green, A.; Hoffmann, G.; Cooper, A. Beachrock: A tool for reconstructing relative sea level in the far-field. *Mar. Geol.* **2015**, *362*, 1–16. [CrossRef]
18. Holail, H.; Rashed, M. Stable isotopic composition of carbonate cemented recent beachrock along the Mediterranean and the Red Sea coasts of Egypt. *Mar. Geol.* **1992**, *106*, 141–148. [CrossRef]
19. Kelletat, D. Beachrock as sea level indicator? Remarks from a geomorphological point of view. *J. Coast. Res.* **2006**, *22*, 1555–1564. [CrossRef]
20. Vousdoukas, M.I.; Velegrakis, A.F.; Plomaritis, T.A. Beachrock occurrence, characteristics, formation mechanisms and impacts. *Earth-Sci. Rev.* **2007**, *85*, 23–46. [CrossRef]
21. Erginal, A.E.; Kıyak, N.G.; Öztürk, B. Investigation of beachrock using microanalyses and OSL dating: A case study from Bozcaada Island, Turkey. *J. Coast. Res.* **2010**, *26*, 350–358. [CrossRef]
22. Danjo, T.; Kawasaki, S. Formation mechanisms of beachrocks in Okinawa and Ishikawa, Japan, with a focus on cements. *Mater. Trans.* **2014**, *55*, 493–500. [CrossRef]
23. Júnior, A.V.; Paes, B.C.; Vieira, M.M.; Sial, A.N.; Neumann, V.H. Diagenesis of Holocene beachrock in northeastern Brazil: Petrology, isotopic evidence and age. *Quat. Environ. Geosci.* **2018**, *2*, 26–35.
24. Nayanthara, P.G.N.; Dassanayake, A.B.N.; Nakashima, K.; Kawasaki, S. Distribution and cementation characteristics of beachrocks along southern, southwestern and western coast of Sri Lanka. *J. Sediment. Environ.* **2021**, *6*, 93–106. [CrossRef]
25. Bathurst, R.G.C. *Carbonate Sediments and Their Diagenesis. Developments in Sedimentology 12*; Elsevier: Amsterdam, The Netherlands, 1975; p. 658.
26. Milliman, J.D. *Marine Carbonates. Part 1, Recent Sedimentary Carbonates*; Springer: New York, NY, USA, 1974; p. 375.
27. Moore, C.H.; Billings, G.K. Preliminary model of beachrock cementation, Grand Cayman Island, B.W.I. In *Carbonate Cements*; Bricker, O.P., Ed.; Johns Hopkins University Press: Baltimore, MD, USA, 1971; pp. 41–43.
28. Hanor, J.S. Precipitation of beachrock cements: Mixing of marine and meteoric waters vs. CO_2-degassing. *J. Sediment. Petrol.* **1978**, *48*, 489–501.
29. Neumeier, U. Experimental modelling of beachrock cementation under microbial influence. *Sediment. Geol.* **1999**, *126*, 35–46. [CrossRef]
30. Webb, G.E.; Jell, J.S.; Baker, J.C. Cryptic intertidal microbialites in beachrock, Heron Island, Great Barrier Reef: Implications for the origin of microcrystalline beachrock cement. *Sediment. Geol.* **1999**, *126*, 317–334. [CrossRef]
31. Wiles, E.; Green, A.N.; Cooper, J.A.G. Rapid beachrock cementation on a South African beach: Linking morphodynamics and cement style. *Sediment. Geol.* **2018**, *378*, 13–18. [CrossRef]
32. Al-Ramadan, K. Diagenesis of Holocene beachrocks: A comparative study between the Arabian Gulf and the Gulf of Aqaba, Saudi Arabia. *Arab. J. Geosci.* **2014**, *7*, 4933–4942. [CrossRef]
33. Ghandour, I.M.; Al-Washmi, H.A.; Bantan, R.A.; Gadallah, M.M. Petrographical and petrophysical characteristics of asynchronous beachrocks along Al-Shoaiba Coast, Red Sea, Saudi Arabia. *Arab. J. Geosci.* **2014**, *7*, 355–365. [CrossRef]
34. Koeshidayatullah, A.; Al-Ramadan, K. Unraveling cementation environment and patterns of Holocene beachrocks in the Arabian Gulf and the Gulf of Aqaba: Stable isotope approach. *Geol. Q.* **2014**, *58*, 207–216. [CrossRef]
35. Haredy, R.A.; Ghandour, I.M.; Erginal, A.E.; Bozcu, M. Beachrock cementation patterns along the Gulf of Aqaba coast, Saudi Arabia. *Arab. J. Sci. Eng.* **2019**, *44*, 479–487. [CrossRef]
36. Mannaa, A.A.; Haredy, R.A.; Ghandour, I.M. Beachrock as a Paleoshoreline Indicator: Example from Wadi Al-Hamd, South Al-Wajh, Saudi Arabia. *J. Mar. Sci. Eng.* **2021**, *9*, 984. [CrossRef]
37. DeMenocal, P.; Ortiz, J.; Guilderson, T.; Sarnthein, M. Abrupt onset and termination of the African humid period: Rapid climate responses to gradual insolation forcing. *Quat. Sci. Rev.* **2000**, *19*, 347–361. [CrossRef]
38. Mitrovica, J.X.; Milne, G.A. On the origin of late Holocene sea level highstands within equatorial ocean basins. *Quat. Sci. Rev.* **2002**, *21*, 2179–2190. [CrossRef]

39. Jado, A.R.; Zötl, J.G. *Quaternary Period in Saudi Arabia*; Springer: Berlin/Heidelberg, Germany, 1984; Volume 2, p. 360.
40. Ritchie, J.C.; Eyles, C.H.; Haynes, C.V. Sediment and pollen evidence for an early to mid-Holocene humid period in the eastern Sahara. *Nature* **1985**, *314*, 352–355. [CrossRef]
41. Bailey, G. The Red Sea, coastal landscapes, and hominin dispersals. In *The Evolution of Human Populations in Arabia*; Petraglia, M.D., Rose, J.I., Eds.; Springer: Berlin/Heidelberg, Germany, 2010; pp. 15–37.
42. Engel, M.; Matter, A.; Parker, A.G.; Parton, A.; Petraglia, M.D.; Preston, G.; Preusser, F. Lakes or wetlands? A comment on "The middle Holocene climatic records from Arabia: Reassessing lacustrine environments, shift of ITCZ in Arabian Sea, and impacts of the southwest Indian and African monsoons" by Enzel et al. *Glob. Planet. Chang.* **2017**, *148*, 258–267. [CrossRef]
43. Biton, E.; Gildor, H.; Trommer, G.; Siccha, M.; Kucera, M.; van der Meer, M.T.; Schouten, S. Sensitivity of Red Sea circulation to monsoonal variability during the Holocene: An integrated data and modeling study. *Paleoceanography* **2010**, *25*, PA4209. [CrossRef]
44. Arz, H.W.; Lamy, F.; Pätzold, J.; Müller, P.J.; Prins, M. Mediterranean moisture source for an early-Holocene humid period in the northern Red Sea. *Science* **2003**, *300*, 118–121. [CrossRef]
45. Lézine, A.M.; Robert, C.; Cleuziou, S.; Inizan, M.L.; Braemer, F.; Saliège, J.F.; Sylvestre, F.; Tiercelin, J.J.; Crassard, R.; Méry, S.; et al. Climate change and human occupation in the southern Arabian lowlands during the last deglaciation and the Holocene. *Glob. Planet. Chang.* **2010**, *72*, 412–428. [CrossRef]
46. Morcos, S.A. Physical and chemical oceanography of the Red Sea. *Oceanogr. Mar. Biol. Annu. Rev.* **1970**, *8*, 73–202.
47. Sofianos, S.S.; Johns, W.E. An oceanic general circulation model (OGCM) investigation of the Red Sea circulation, 1. Exchange between the Red Sea and the Indian Ocean. *J. Geophys. Res. Ocean.* **2002**, *107*, 17-1–17-11. [CrossRef]
48. Manaa, A.A.; Jones, B.G.; McGregor, H.V.; Zhao, J.X.; Price, D.M. Dating Quaternary raised coral terraces along the Saudi Arabian Red Sea coast. *Mar. Geol.* **2016**, *374*, 59–72. [CrossRef]
49. Fouda, M.M.; Gerges, M.A. *Implication of Climate Change in the Red Sea and Gulf of Aden Region: An Overview*; United Nations Environment Programme, Regional Seas Reports and Studies: Nairobi, Kenya, 1994.
50. Shanas, P.R.; Aboobacker, V.M.; Albarakati, A.M.A.; Zubier, K.M. Superimposed wind-waves in the Red Sea. *Ocean. Eng.* **2017**, *138*, 9–22. [CrossRef]
51. Langodan, S.; Cavaleri, L.; Pomaro, A.; Portilla, J.; Abualnaja, Y.; Hoteit, I. Unraveling climatic wind and wave trends in the Red Sea using wave spectra partitioning. *J. Clim.* **2018**, *31*, 1881–1895. [CrossRef]
52. Langodan, S.; Cavaleri, L.; Viswanadhapalli, Y.; Hoteit, I. The Red Sea: A natural laboratory for wind and wave modeling. *J. Phys. Oceanogr.* **2014**, *44*, 3139–3159. [CrossRef]
53. Jiang, H.; Farrar, J.T.; Beardsley, R.C.; Chen, R.; Chen, C. Zonal surface wind jets across the Red Sea due to mountain gap forcing along both sides of the Red Sea. *Geophys. Res. Lett.* **2009**, *36*, L19605. [CrossRef]
54. Kemp, A.C.; Horton, B.; Donnelly, J.P.; Mann, M.E.; Vermeer, M.; Rahmstorf, S. Climate related sea-level variations over the past two millennia. *Proc. Natl. Acad. Sci. USA* **2011**, *108*, 11017–11022. [CrossRef] [PubMed]
55. Woodroffe, C.D.; Webster, J.M. Coral reefs and sea-level change. *Mar. Geol.* **2014**, *352*, 248–267. [CrossRef]
56. Lambeck, K.; Rouby, H.; Purcell, A.; Sun, Y.; Sambridge, M. Sea level and global ice volumes from the last glacial maximum to the Holocene. *Proc. Natl. Acad. Sci. USA* **2014**, *111*, 15296–15303. [CrossRef] [PubMed]
57. Brooke, B.P.; Huang, Z.; Nicholas, W.A.; Oliver, T.S.; Tamura, T.; Woodroffe, C.D.; Nichol, S.L. Relative sea-level records preserved in Holocene beach-ridge strandplains—An example from tropical northeastern Australia. *Mar. Geol.* **2019**, *411*, 107–118. [CrossRef]
58. Dougherty, A.J.; Thomas, Z.A.; Fogwill, C.; Hogg, A.; Palmer, J.; Rainsley, E.; Williams, A.N.; Ulm, S.; Rogers, K.; Jones, B.G.; et al. Redating the earliest evidence of the mid-Holocene relative sea-level highstand in Australia and implications for global sea-level rise. *PLoS ONE* **2019**, *14*, e0218430. [CrossRef] [PubMed]
59. Rushby, G.T.; Richards, G.T.; Gehrels, W.R.; Anderson, W.P.; Bateman, M.D.; Blake, W.H. Testing the mid-Holocene relative sea-level highstand hypothesis in north Wales, United Kingdom. *Holocene* **2019**, *29*, 1491–1502. [CrossRef]
60. Shaked, Y.; Marco, S.; Lazar, B.; Stein, M.; Cohen, C.; Sass, E.; Agnon, A. Late Holocene shorelines at the Gulf of Aqaba: Migrating shorelines under conditions of tectonic and sea level stability. *Eur. Geosci. Union Stephan Mueller Spec. Publ. Ser.* **2002**, *2*, 1–7. [CrossRef]
61. Hein, C.J.; FitzGerald, D.M.; Milne, G.A.; Bard, K.; Fattovich, R. Evolution of a Pharaonic harbor on the Red Sea: Implications for coastal response to changes in sea level and climate. *Geology* **2011**, *39*, 687–690. [CrossRef]
62. Al-Mikhlafi, A.S.; Hibbert, F.D.; Edwards, L.R.; Cheng, H. Holocene relative sea-level changes and coastal evolution along the coastlines of Kamaran Island and As-Salif Peninsula, Yemen, southern Red Sea. *Quat. Sci. Rev.* **2021**, *252*, 106719. [CrossRef]
63. Behairy, A.K.A.; Durgaprasada Rao, N.V.N.; El-Shater, A. A siliciclastic coastal sabkha, Red Sea coast, Saudi Arabia. *J. King Abdulaziz Univ. Mar. Sci.* **1991**, *2*, 65–77. [CrossRef]
64. Ghandour, I.M.; Haredy, R.A. Facies analysis and sequence stratigraphy of Al-Kharrar Lagoon coastal sediments, Rabigh Area, Saudi Arabia: Impact of sea level and climate changes on coastal evolution. *Arab. J. Sci. Eng.* **2019**, *44*, 505–520. [CrossRef]
65. Ghandour, I.M.; Majeed, J.; Al-Zubieri, A.G.; Mannaa, A.A.; Aljahdali, M.H.; Bantan, R.A. Late Holocene Red Sea coastal evolution: Evidence from shallow subsurface sedimentary facies, north Al-Wajh, Saudi Arabia. *Thalass. Int. J. Mar. Sci.* **2021**, *37*, 1–12.

66. Ghandour, I.M.; Al-Zubieri, A.G.; Basaham, A.S.; Mannaa, A.A.; Al-Dubai, T.A.; Jones, B.G. Mid-late Holocene paleoenvironmental and sea level reconstruction on the Al Lith Red Sea coast, Saudi Arabia. *Front. Mar. Sci.* **2021**, *8*, 677010. [CrossRef]
67. Abu-Zied, R.H.; Bantan, R.A. Palaeoenvironment, palaeoclimate and sea-level changes in the Shuaiba Lagoon during the late Holocene (last 3.6 ka), eastern Red Sea coast, Saudi Arabia. *Holocene* **2015**, *25*, 1301–1312. [CrossRef]
68. Bantan, R.A.; Abu-Zied, R.H.; Al-Dubai, T.A. Late Holocene environmental changes in a sediment core from Al-Kharrar Lagoon, eastern Red Sea Coast, Saudi Arabia. *Arab. J. Sci. Eng.* **2019**, *44*, 6557–6570. [CrossRef]
69. Basaham, A.S.; El Sayed, M.A.; Ghandour, I.M.; Masuda, H. Geochemical background for the Saudi Red Sea coastal systems and its implication for future environmental monitoring and assessment. *Environ. Earth Sci.* **2015**, *74*, 4561–4570. [CrossRef]
70. Basaham, A.S.; Ghandour, I.M.; Haredy, R. Controlling factors on the geochemistry of Al-Shuaiba and Al-Mejarma coastal lagoons, Red Sea, Saudi Arabia. *Open Geosci.* **2019**, *11*, 426–439. [CrossRef]
71. Lisitzin, E. *Sea Level Changes*; Elsevier: Amsterdam, The Netherlands, 1974.
72. Johnson, P.R. *Explanatory Notes to the Map of Proterozoic Geology of Western Saudi Arabia*; Technical Report; Saudi Geological Survey: Jeddah, Saudi Arabia, 2006.
73. Greenwood, W.R.; Stoeser, D.B.; Fleck, R.J.; Stacey, J.S. *Late Proterozoic Island-Arc Complexes and Tectonic Belts in the Southern Part of the Arabian Shield, Kingdom of Saudi Arabia*; Open-File Report, 1982-83-296; Ministry of Petroleum and Mineral Resources, Deputy Ministry for Mineral Resources: Jeddah, Saudi Arabia, 1982.
74. Goldsmith, J.R.; Graf, D.L.; Heard, H.C. Lattice constants of the calcium-magnesium carbonates. *Am. Mineral.* **1961**, *46*, 453–457.
75. Craig, H. Isotopic standards for carbon and oxygen correction factors for mass spectrometric analysis of carbon dioxide. *Geochim. Cosmochim. Acta* **1957**, *12*, 133–149. [CrossRef]
76. Keith, M.L.; Weber, J.N. Carbon and oxygen isotopic composition of selected limestones and fossils. *Geochim. Cosmochim. Acta* **1964**, *28*, 1787–1816. [CrossRef]
77. Reading, H.G. Clastic coast. In *Sedimentary Environments: Processes, Facies and Stratigraphy*; Reading, H.G., Ed.; Blackwell Science: Oxford, UK, 1996; pp. 154–231.
78. Lessa, G.C.; Angulo, R.J.; Giannini, P.C.; Arau´jo, A.D. Stratigraphy and Holocene evolution of a regressive barrier in south Brazil. *Mar. Geol.* **2000**, *165*, 87–108. [CrossRef]
79. González-Villanueva, R.; Pérez-Arlucea, M.; Costas, S.; Bao, R.; Otero, X.L.; Goble, R. 8000 years of environmental evolution of barrier-lagoon systems emplaced in coastal embayments (NW Iberia). *Holocene* **2015**, *25*, 1786–1801. [CrossRef]
80. Bezzi, A.; Casagrande, G.; Martinucci, D.; Pillon, S.; del Grande, C.; Fontolan, G. Modern sedimentary facies in a progradational barrier-spit system: Goro lagoon, Po delta, Italy. *Estuar. Coast. Shelf Sci.* **2019**, *227*, 106323. [CrossRef]
81. McCubbin, D.G. Barrier-island and strand-plain facies. In *Sandstone Depositional Environments*; Scholle, P.A., Darwin Spearing, D., Eds.; AAPG Memoir: Tulsa, OK, USA, 1982; Volume 31, pp. 247–279.
82. Clifton, H.E. A re-examination of facies models for clastic shorelines. In *Facies Models Revisited*; Posamentier, H.G., Walker, R.G., Eds.; SEPM Special Publication: Tulsa, OK, USA, 2006; Volume 84, pp. 293–337.
83. Lindhorst, S.; Betzler, C.; Hass, H.C. The sedimentary architecture of a Holocene barrier spit (Sylt, German Bight): Swash-bar accretion and storm erosion. *Sediment. Geol.* **2008**, *206*, 1–16. [CrossRef]
84. Van Heteren, S. Barrier systems. In *Coastal Environments and Global Change*; Masselink, G., Gehrels, R., Eds.; John Wiley and Sons: Hoboken, NJ, USA, 2015; pp. 194–226.
85. Sousa, C.; Boski, T.; Pereira, L. Holocene evolution of a barrier island system, Ria Formosa, south Portugal. *Holocene* **2019**, *29*, 64–76. [CrossRef]
86. FitzGerald, D.M.; Rosen, P.S. *Glaciated Coasts*; Academic Press: London, UK, 1987.
87. FitzGerald, D.; van Heteren, S. Classification of paraglacial barrier systems: Coastal New England, U.S.A. *Sedimentology* **1999**, *46*, 1083–1108. [CrossRef]
88. Sloss, C.R.; Jones, B.G.; Murray-Wallace, C.V.; McClennen, C.E. Holocene sea level fluctuations and the sedimentary evolution of a barrier estuary: Lake Illawarra, New South Wales, Australia. *J. Coast. Res.* **2005**, *21*, 943–959. [CrossRef]
89. Joury, M.R.F.; James, N.P.; James, C. Nearshore cool-water carbonate sedimentation and provenance of Holocene calcareous strandline dunes, southeastern Australia. *Aust. J. Earth Sci.* **2018**, *65*, 221–242. [CrossRef]
90. Durgaprasada Rao, N.V.N.; Behairy, A.K.A. Intertidal conglomerate south of Yanbu—An episodic clastic deposit in the eastern Red Sea. *Palaeogeogr. Palaeoclimatol. Palaeoecol.* **1987**, *58*, 221–228. [CrossRef]
91. Fruergaard, M.; Tessier, B.; Poirier, C.; Mouazé, D.; Weill, P.; Noël, S. Depositional controls on a hypertidal barrier-spit system architecture and evolution, Pointe du Banc spit, north-western France. *Sedimentology* **2020**, *67*, 502–533. [CrossRef]
92. Flemming, B.W. Siliciclastic back-barrier tidal flats. In *Principles of Tidal Sedimentology*; Davis, R.A., Dalrymple, R.W., Eds.; Springer: Berlin/Heidelberg, Germany, 2012; pp. 231–267.
93. Storms, J.E.A. Event-based stratigraphic simulation of wave-dominated shallow-marine environments. *Mar. Geol.* **2003**, *199*, 83–100. [CrossRef]
94. Aagaard, T.; Davidson-Arnott, R.; Greenwood, B.; Nielsen, J. Sediment supply from shoreface to dunes: Linking sediment transport measurements and long-term morphological evolution. *Geomorphology* **2004**, *60*, 205–224. [CrossRef]
95. Snedden, J.W.; Nummedal, D. Coherence of surf zone and shelf current flow on the Texas (USA) coastal margin: Implications for interpretation of paleo-current measurements in ancient coastal sequences. *Sediment. Geol.* **1990**, *67*, 221–236. [CrossRef]

96. Reineck, H.E.; Singh, I.B. *Depositional Sedimentary Environments with Reference to Terrigenous Clastics*; Springer: Berlin/Heidelberg, Germany, 1980.
97. Klein, D. *Sandstone Depositional Models for Exploration for Fossil Fuels*; International Human Resources Development Corporation: Boston, MA, USA, 1982.
98. Fox, W.T.; Davis, R.J. Seasonal variation in beach erosion and sedimentation on the Oregon Coast. *Geol. Soc. Am. Bull.* **1978**, *89*, 1541–1549. [CrossRef]
99. Peltier, W.R. On eustatic sea level history: Last Glacial Maximum to Holocene. *Quat. Sci. Rev.* **2002**, *21*, 377–396. [CrossRef]
100. Clemmensen, L.B.; Andreasen, F.; Nielsen, S.T.; Sten, E. The late Holocene coastal dunefield at Vejers, Denmark: Characteristics, sand budget and depositional dynamics. *Geomorphology* **1996**, *17*, 79–98. [CrossRef]
101. Psuty, N.P.; Eugénia, M.; Moreira, S.A. Holocene sedimentation and sea level rise in the Sado Estuary, Portugal. *J. Coast. Res.* **2000**, *16*, 125–138.
102. Walker, R.G.; James, N.P. *Facies Models Response to Sea Level Change*, 2nd ed.; Geological Association of Canada: St. John's, NS, Canada, 1992; p. 409.
103. De Falco, G.; Antonioli, F.; Fontolan, G.; lo Presti, V.; Simeone, S.; Tonielli, R. Early cementation and accommodation space dictate the evolution of an overstepping barrier system during the Holocene. *Mar. Geol.* **2015**, *369*, 52–66. [CrossRef]
104. Moore, C.H. *Carbonate Diagenesis and Porosity*; Elsevier: Amsterdam, The Netherlands, 1989.
105. Longman, M.W. Carbonate diagenetic textures from near surface diagenetic environments. *Am. Assoc. Pet. Geol. Bull.* **1980**, *64*, 461–487.
106. James, N.P.; Choquette, P.W. Limestone: The sea floor diagenetic environment. In *Diagenesis*; McIlreath, I., Morrow, D., Eds.; Canada Geological Association of Canada Reprint Series: St John's, ND, Canada, 1990; pp. 13–34.
107. Scholle, P.A.; Ulmer-Scholle, D.S. A color guide to the petrography of carbonate rocks: Grains, textures, porosity, diagenesis. *Am. Assoc. Pet. Geol. Mem.* **2003**, *77*, 1–474.
108. Vieira, M.M.; Sial, A.N.; de Ros, L.F.; Morad, S. Origin of Holocene beachrock cements in northeastern Brazil: Evidence from carbon and oxygen isotopes. *J. South Am. Earth Sci.* **2017**, *79*, 401–408. [CrossRef]
109. Hopley, D. Beachrock as sea level indicator. In *Sea Level Research*; van de Plassche, O., Ed.; Great Yarmouth: Galliard Printers, UK, 1986; pp. 157–173.
110. Holail, H.M.; Shaaban, M.N.; Mansour, A.S. Cementation of Holocene beachrock in the Aqaba and the Arabian Gulfs: Comparative study. *Carbonates Evaporites* **2004**, *19*, 142–150. [CrossRef]
111. Hillgärtner, H.; Dupraz, C.; Hug, W. Microbially induced cementation of carbonate sands: Are micritic meniscus cements good indicators of vadose diagenesis? *Sedimentology* **2001**, *48*, 117–131. [CrossRef]
112. Calvet, F.; Cabrera, M.C.; Carracedo, J.C.; Mangas, J.; Pérez-Torrado, F.J.; Recio, C.; Travé, A. Beachrocks from the island of La Palma (Canary Islands, Spain). *Mar. Geol.* **2003**, *197*, 75–93. [CrossRef]
113. Friedman, G.M. Climatic significance of Holocene beachrock sites along shorelines of the Red Sea. *Am. Assoc. Pet. Geol. Bull.* **2005**, *89*, 849–852. [CrossRef]
114. Vieira, M.M.; de Ros, L.F. Cementation patterns and genetic implications of Holocene beachrocks from northeastern Brazil. *Sediment. Geol.* **2006**, *192*, 207–230. [CrossRef]
115. Hoefs, J. *Stable Isotope Geochemistry*; Springer: Berlin/Heidelberg, Germany, 1997.
116. Woodroffe, C.D. *Coasts: Form, Process, and Evolution*; Cambridge University Press: Cambridge, UK, 2003.
117. Dullo, W.C.; Montaggioni, L. Modern Red Sea coral reefs: A review of their morphologies and zonation. In *Sedimentary and Tectonic Evolution of Rift Basins–The Red Sea-Gulf of Aden*; Purser, B.H., Bosence, D.W.J., Eds.; Springer: Berlin/Heidelberg, Germany, 1998; pp. 583–594.